Towards Thermal-Aware Humanoid Locomotion: Estimating Unobserved Winding Temperatures

Eunwoo Song[*1,2] Sangmin Lee[*1†] Yeonji Kim[1] Heewon Kim[‡1,2]
[1]Soongsil University [2]Kairoba
song200348@soongsil.ac.kr, sm32289@gmail.com, yeonpond02@soongsil.ac.kr, hwkim@ssu.ac.kr

Abstract

Sustained humanoid locomotion is bounded by progressive torque degradation from motor heating, and failure is driven by the unobservable winding temperature rather than the measurable housing. First-order models cannot represent the winding state, while standard second-order LPTNs assume embedded winding sensors and treat each actuator in isolation, both invalid on humanoid servo-integrated actuators. We adapt the coupled second-order LPTN with physically-informed regularizers derived from non-destructive teardown of commercial servos and an inter-motor coupling term for shared housings and PLA-frame conduction, identified from only the integer-quantized housing temperature. On the ToddlerBot platform with 30 actuators, the identified model recovers the unobserved winding state with physically consistent behavior across 10 walk sessions. Lacking an embedded winding sensor, we validate the estimate not by pointwise accuracy but by physical consistency and by an independent resistance-thermometry measurement on the load-bearing joints, providing a foundation for thermal-aware locomotion policies.

1. Introduction

Reinforcement learning has enabled humanoid robots to acquire agile locomotion through large-scale simulation training [4, 21], but sustained real-world deployment exposes a failure mode that standard physics simulators [14, 22] do not capture: progressive torque degradation from motor heating. In humanoids that pack tens of compact actuators into a single body [19], every step injects Joule heat that monotonically shrinks the torque envelope through rising winding resistance [13, 20], directly bounding how long a humanoid can walk before failure. Existing fault-tolerant control predominantly targets discrete events such as joint locking via domain randomization [8, 11, 12], absorbing thermal effects into a fixed derating coefficient [6, 20] that erases actuator-specific physics. Motor-control estimators [1, 9, 10] assume dedicated winding sensors, while their robotics adaptations [7, 16] lean on single-actuator manufacturer thermal constants, neither available on the compact servo-integrated actuators here, where only an integer-quantized housing temperature is exposed.

To account for these conditions, we adapt the coupled second-order Lumped Parameter Thermal Network (LPTN) [1, 15] with two practical adjustments tailored to humanoid hardware. First, a physical prior on the winding thermal capacitance is reverse-engineered from non-destructive disassembly of commercial servos [18], while the winding-housing thermal resistance is set to a physically-consistent order of magnitude, together replacing the embedded-thermistor assumption this hardware does not satisfy. Second, an inter-motor coupling term models shared mechanical housings (8 pairs in ToddlerBot [19]) and PLA-frame conduction between kinematic neighbors, which standard single-motor LPTNs omit.

2. Thermal Parameter Identification

Model. Each actuator is a coupled second-order LPTN with a winding (*core*) node and a housing node, augmented with an inter-motor coupling term [1, 5, 15] (Fig. 1). The measured current I_i and the temperature-dependent winding resistance $R_{e,i}(\widehat{T}_{w,i})$ [18] inject Joule heating at the core, which flows winding→housing→ambient T_a with a board term $P_{b,i}$; the constitutive expressions appear in Fig. 1. The inter-motor flux $\dot{Q}_{\mathrm{cpl},i}$ adds a rigid housing-pair path ($R_{ch,i}$, partner $p(i)$) and a PLA kinematic-neighbor path ($R_{ck,i}$, K_i neighbors); because the neighbor housing $\bar{T}_{h,\mathcal{N}(i)}$ entering this term is itself *measured*, the 30 per-motor fits decouple and are solved independently [3, 19, 23]. Only the housing $T_{h,i}$ is measured while the winding $\widehat{T}_{w,i}$ stays hidden, so the winding pole is unobservable from housing data alone and a physical constraint is required

---

[*]Equal contribution
[†]Now at Qualcomm
[‡]Corresponding author

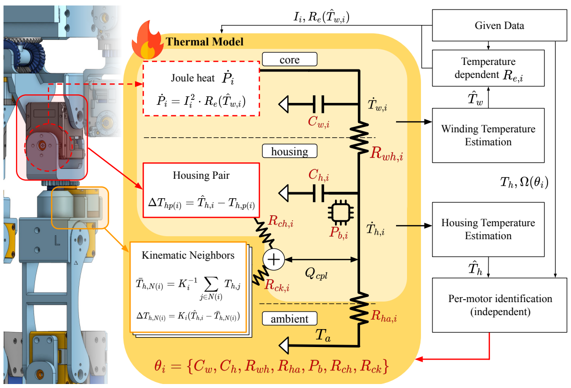

Figure 1. Coupled second-order LPTN per actuator: Joule heating at the winding (*core*) node, driven by I_i and $R_{e,i}(\widehat{T}_{w,i})$, flows winding→housing→ambient ($R_{wh,i}$, $R_{ha,i}$) plus two inter-motor paths (housing-pair $R_{ch,i}$, PLA-neighbor $R_{ck,i}$). Only $T_{h,i}$ is measured; $\widehat{T}_{w,i}$ is hidden.

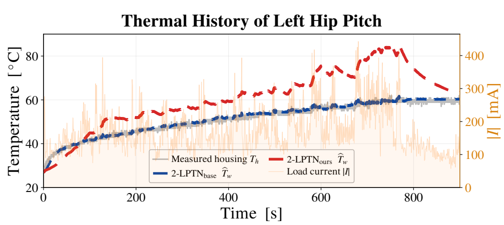

Figure 2. Thermal history of one representative actuator (left hip pitch, one walk session); only T_h is measured. The 2-LPTN$_{\text{base}}$ winding $\widehat{T}_w$ collapses onto the housing trace (mean gap 0.7°C), whereas 2-LPTN$_{\text{ours}}$ exposes a $+22$°C winding over-temperature the housing misses.

to identify it; the free parameters per motor are $\theta_i = \{C_w, C_h, R_{wh}, R_{ha}, P_b, R_{ch}, R_{ck}\}$ (7 each, 210 total).

Per-motor identification. Each θ_i is identified *independently* by forward-integrating the LPTN to predict $\widehat{T}_{h,i}(\theta_i)$ and minimizing

$$\min_{\theta_i} \ \frac{1}{N} \sum_{s,k} \big(T_{h,i}[k] - \widehat{T}_{h,i}(\theta_i; s)[k]\big)^2 \ + \ \lambda\, \Omega(\theta_i), \quad (1)$$

where N is the per-motor sample count, so both terms share a common per-sample scale and a single weight λ trades data fidelity against the regularizer. The data-fit term is the mean squared housing residual, and the Tikhonov regularizer $\Omega(\theta_i)$ supplies the missing physical constraint by drawing the identifiability-critical subset $\{C_w, R_{wh}, R_{ha}\}$ toward physically-motivated references (motor mass, multi-path conduction, a one-time cold-start; derived in Sec. 3); the remaining parameters are bounded only, and trust-region least-squares [2] converges in minutes.

3. Experiments

Data collection. The regularizer references are physically grounded, not assumed: C_w from a non-destructive teardown [18], R_{wh} to the order of magnitude of winding–housing conduction [1, 3], and R_{ha} from a one-time cold-start [23]. Models are identified on heated random excitation and evaluated out-of-distribution on 10 held-out walk sessions across the 30 actuators.

Table 1. Housing RMSE (avg/med/worst over 30 motors, 10 held-out walk sessions) and peak winding $\widehat{T}_w$ (legs, mean±std).

Model	RMSE [°C]			Peak $\widehat{T}_w$
	Avg.	Med.	Worst	(legs) [°C]
1-LPTN$_{\text{base}}$	11.12	6.02	60.31	–
1-LPTN$_{Q_{\text{cpl}}}$	2.28	2.25	5.28	–
2-LPTN$_{\text{base}}$	2.09	1.86	4.54	115 ± 97
2-LPTN$_{\text{ours}}$	2.30	2.17	4.75	80 ± 29

Quantitative results. In Tab. 1, 1-LPTN$_{\text{base}}$ (no inter-motor coupling) is catastrophic (Avg. 11.1°C, Worst 60.3°C), confirming that coupling is essential on a dense platform. With coupling, 1-LPTN$_{Q_{\text{cpl}}}$ matches the housing well (2.28°C), and 2-LPTN$_{\text{base}}$ attains essentially the same housing accuracy (2.09°C); yet its winding state is unconstrained, spreading to 115 ± 97°C with excursions beyond 500°C, i.e. without Ω the winding pole is unidentifiable. At matched housing accuracy (2.30°C, on par with 1-LPTN$_{Q_{\text{cpl}}}$), Ω sharply contracts the winding estimate to 80 ± 29°C, a far more constrained hidden state than the unconstrained baseline, at no cost in housing fidelity (Fig. 2). The fitted inter-motor resistances separate by an order of magnitude: motors sharing a housing ($R_{ch} \sim 3$ K/W) couple far more strongly than neighbors linked only through the 3D-printed PLA frame ($R_{ck} \sim 30$ K/W), consistent with the platform's construction [19] and confirming the coupling term captures real conduction paths.

Independent validation. The winding–housing resistance R_{wh} enters Ω only as an order-of-magnitude prior ($\sim$ 25 K/W). On the high-load knee and ankle actuators, where the resistive voltage drop dominates the back-EMF, independent resistance thermometry [17] (coil resistance from the logged voltage and current with the back-EMF removed using the rated motor constant, then converted to temperature via copper's temperature coefficient of resistance; 247 windows) places R_{wh} near 10 K/W and gives a winding-to-housing gap of up to 39°C, indicating that the recovered state is physically real. Because R_{wh} is not observable from the housing, its prior leaves the housing fit essentially unchanged (Wilcoxon signed-rank test, $p = 0.17$), so the winding pole is limited by identifiability, not by data.

4. Limitation and future work

Because direct winding-temperature ground truth is unavailable, we evaluate physical consistency rather than pointwise temperature accuracy. Our method is evaluated in a single platform and policy, and cross-embodiment evaluation across robots and controllers remains future work.

Acknowledgements

This research was supported by the MSIT(Ministry of Science and ICT), Korea, under the Advanced GPU Utilization Support Program, the National Program for Excellence in SW (2024-0-00071), and the graduate school support program (IITP-2026-RS-2024-00430997, IITP-2026-RS-2024-00426853) supervised by the IITP (Institute of Information & communications Technology Planning & evaluation) and the National Research Foundation of Korea (NRF) grants funded by the Korea government (MSIT) (RS-2025-24803335) and the Ministry of Education (MOE) for the G-LAMP program (RS-2025-25441317), and Seoul Metropolitan Government for the RISE program (2025-RISE-01-020-04), and Basic Science Research Program (RS-2021-NR060140).

References

[1] Aldo Boglietti, Enrico Carpaneto, Marco Cossale, and Silvio Vaschetto. Stator-winding thermal models for short-time thermal transients: Definition and validation. *IEEE Trans. Ind. Electron.*, 63(5):2713–2721, 2016. 1, 2

[2] Mary Ann Branch, Thomas F. Coleman, and Yuying Li. A subspace, interior, and conjugate gradient method for large-scale bound-constrained minimization problems. *SIAM J. Sci. Comput.*, 21(1):1–23, 1999. 2

[3] Georgios D. Demetriades, Hector Zelaya de la Parra, Erik Andersson, and Henrik Olsson. A real-time thermal model of a permanent-magnet synchronous motor. *IEEE Trans. Power Electron.*, 25(2):463–474, 2010. 1, 2

[4] Shangding Gu, Long Yang, Yali Du, Guang Chen, Florian Walter, Jun Wang, Yaodong Yang, and Alois Knoll. A review of safe reinforcement learning: Methods, theory and applications. *IEEE Trans. Pattern Anal. Mach. Intell.*, 46 (12):11216–11235, 2024. 1

[5] Mathieu Guilbert, Ludovic Joly, and Pierre-Brice Wieber. Optimization of complex robot applications under real physical limitations. *Int. J. Robot. Res.*, 27(5):629–644, 2008. 1

[6] Steven Jens Jorgensen, James Holley, Frank Mathis, Joshua S. Mehling, and Luis Sentis. Thermal recovery of multi-limbed robots with electric actuators. *IEEE Robot. Autom. Lett.*, 4(2):1077–1084, 2019. 1

[7] Kento Kawaharazuka, Naoki Hiraoka, Kei Tsuzuki, Moritaka Onitsuka, Yuki Asano, Kei Okada, Koji Kawasaki, and Masayuki Inaba. Estimation and control of motor core temperature with online learning of thermal model parameters: Application to musculoskeletal humanoids. *IEEE Robot. Autom. Lett.*, 5(3):4273–4280, 2020. 1

[8] Mincheol Kim, Ukcheol Shin, and Jung-Yup Kim. Learning quadrupedal locomotion with impaired joints using random joint masking. In *IEEE Int. Conf. Robot. Autom.*, pages 9751–9757, 2024. 1

[9] Wilhelm Kirchgässner, Oliver Wallscheid, and Joachim Böcker. Estimating electric motor temperatures with deep residual machine learning. *IEEE Trans. Power Electron.*, 36 (7):7480–7488, 2021. 1

[10] Nicholas Krause, Daniel Sossong, and Ian P. Brown. Grey-box thermal parameter identification of electric machine stators. In *IEEE Energy Convers. Congr. Expo.*, pages 5447–5454, 2024. 1

[11] Joonho Lee, Jemin Hwangbo, and Marco Hutter. Robust recovery controller for a quadrupedal robot using deep reinforcement learning. *arXiv preprint arXiv:1901.07517*, 2019. 1

[12] Sanghun Lee, I Made Aswin Nahrendra, Donghoon Lee, Byeongho Yu, Minho Oh, Hyun Lee, and Hyun Myung. DreamFLEX: Learning fault-aware quadrupedal locomotion controller for anomaly situation in rough terrains. In *IEEE Int. Conf. Robot. Autom.*, pages 16001–16007, 2025. 1

[13] Leroy-Somer. Technical information — motors. Technical Note, Nidec/Leroy-Somer, 2019. 1

[14] Viktor Makoviychuk, Lukasz Wawrzyniak, Yunrong Guo, Michelle Lu, Kier Storey, Miles Macklin, David Hoeller, Nikita Rudin, Arthur Allshire, Ankur Handa, and Gavriel State. Isaac gym: High performance GPU-based physics simulation for robot learning. *Adv. Neural Inform. Process. Syst.*, 2021. 1

[15] P. H. Mellor, D. Roberts, and D. R. Turner. Lumped parameter thermal model for electrical machines of TEFC design. *IEE Proc. B Electr. Power Appl.*, 138(5):205–218, 1991. 1

[16] Daniel Müller. Olaf: Bringing an animated character to life in the physical world. *arXiv preprint arXiv:2512.16705*, 2025. 1

[17] Roel Pantonial, Alan Kilantang, and Bernardino Buenaobra. Real time thermal estimation of a brushed DC motor by a steady-state Kalman filter algorithm in multi-rate sampling scheme. In *IEEE Region 10 Conf. (TENCON)*, pages 1–6, 2012. 2

[18] Tomy Sebastian. Temperature effects on torque production and efficiency of PM motors using NdFeB magnets. *IEEE Trans. Ind. Appl.*, 31(2):353–357, 1995. 1, 2

[19] Haochen Shi, Weizhuo Wang, Shuran Song, and C. Karen Liu. ToddlerBot: Open-source ML-compatible humanoid platform for loco-manipulation. In *Conf. Robot Learn.*, 2025. 1, 2

[20] Akash Singh, Navvab Kashiri, and Nikos Tsagarakis. Thermal control for peak operation of electric robotic actuators. In *Int. Conf. Adv. Robot.*, pages 763–770, 2021. 1

[21] Chen Tang, Ben Abbatematteo, Jiaheng Hu, Rohan Chandra, Roberto Martín-Martín, and Peter Stone. Deep reinforcement learning for robotics: A survey of real-world successes. *arXiv preprint arXiv:2408.03539*, 2024. 1

[22] Emanuel Todorov, Tom Erez, and Yuval Tassa. MuJoCo: A physics engine for model-based control. In *IEEE/RSJ Int. Conf. Intell. Robot. Syst.*, pages 5026–5033, 2012. 1

[23] Oliver Wallscheid and Joachim Böcker. Global identification of a low-order lumped-parameter thermal network for permanent magnet synchronous motors. *IEEE Trans. Energy Convers.*, 31(1):354–365, 2016. 1, 2